γ width of the unbound 5.17 MeV level of ^{14}O and the "hot" CNO cycle

P. B. Fernandez,* E. G. Adelberger, and A. Garcia
Physics Department, University of Washington, Seattle, Washington 98195
(Received 22 May 1989; revised manuscript received 21 August 1989)

We have measured the γ-ray branching ratio Γ_γ/Γ of the unbound 5.17 MeV first excited state in ^{14}O using the ^{12}C(^{3}He,$n\gamma$) reaction at $E_{^3\mathrm{He}}=9.35$ MeV. We detected coincidences between n_1 neutrons populating the ^{14}O state and 5.17 MeV γ rays from its decay, and obtained $\Gamma_\gamma/\Gamma=(7.2\pm3.5)\times10^{-5}$. When combined with the known total width $\Gamma=38.1\pm1.8$ keV, our branching ratio corresponds to $\Gamma_\gamma=2.7\pm1.3$ eV. We use this γ-ray width, together with previously measured nonresonant ^{13}C(p,γ_1) data, to find the ^{13}N(p,γ) reaction rate at astrophysical energies, thereby determining the stellar environments where hydrogen burning through "hot" or β-limited CNO cycle can occur.

I. INTRODUCTION

Hydrogen burning in massive stars proceeds largely through the CNO cycle. In the normal CNO cycle, the principal nuclear reaction sequence converts four hydrogen nuclei into an alpha particle:

$$^{12}\mathrm{C}(p,\gamma)^{13}\mathrm{N}(\beta^+)^{13}\mathrm{C}(p,\gamma)^{14}\mathrm{N}(p,\gamma)^{15}\mathrm{O}(\beta^+)^{15}\mathrm{N}(p,\alpha)^{12}\mathrm{C}.$$

This hydrogen burning process is believed to be the principal source of energy in the core of main sequence stars with mass $M > 2M_\odot$ and temperature T in the range $20\times10^6 \leq T < 10^8$ K.[1,2] In this temperature regime ^{14}N(p,γ) is the slowest of the (p,γ) reactions, and for the typical densities expected in these environments, $\rho \leq 100$ g/cm^3, it is also slower than the β-decay rates of ^{13}N, $\tau = 863$ s, and ^{15}O, $\tau = 176$ s.[1] Under these conditions of density and temperature, the carbon and oxygen isotopes are mostly converted to ^{14}N. The rate of energy generation of the cycle is limited by the ^{14}N(p,γ) rate, and it is therefore very sensitive to the stellar temperature T.

As the temperature increases, the charged particle penetration factors become larger, favoring the proton capture reactions, and the waiting point of the cycle shifts from the ^{14}N(p,γ) reaction to the slowest of the β decays, ^{13}N(β^+). For higher temperatures, in the range $T \approx 1$–2×10^8 K, it is expected that the ^{13}N(p,γ)^{14}O reaction will become faster than the β decay of ^{13}N.[3,4] The cycle then turns into the "hot" or β-limited CNO cycle, where the main sequence of reactions is[5]

$$^{12}\mathrm{C}(p,\gamma)^{13}\mathrm{N}(p,\gamma)^{14}\mathrm{O}(\beta^+)^{14}\mathrm{N}(p,\gamma)^{15}\mathrm{O}(\beta^+)^{15}\mathrm{N}(p,\alpha)^{12}\mathrm{C}.$$

The rate of the cycle is now determined by the β-decay rates of ^{14}O, $\tau = 102$ s, and ^{15}O, $\tau = 176$ s. The shift in the limiting rate to the β decays of ^{14}O and ^{15}O leads to an enhancement of the oxygen isotopes.[5] It also affects the dynamics of the stellar environment, since the rate of energy generation is determined by the faster positron decay rates and is basically temperature independent. The temperature and density conditions required for the "hot" CNO cycle presumably occur in supermassive stars ($M \geq 10^5$–10^8 $M_\odot$), accreting neutron stars, red giants with neutron star cores, and nova and supernova outbursts (see Ref. 6 and references therein).

The "hot" CNO cycle is triggered when the mean lifetime for proton capture on ^{13}N, $\tau_p(^{13}\mathrm{N})$, becomes smaller than the positron decay lifetime, $\tau_{\beta+}(^{13}\mathrm{N})$. The mean lifetime $\tau_p(^{13}\mathrm{N})$ of ^{13}N for interaction with protons is given by[7]

$$\tau_p(^{13}\mathrm{N}) = \left[\rho N_A \frac{X_\mathrm{H}}{A_\mathrm{H}}\langle\sigma v\rangle\right]^{-1},$$

where ρ is the matter density; N_A is Avogadro's number; X_H is the hydrogen fraction by mass; and $A_\mathrm{H} = 1.0078$ is the hydrogen atomic mass number. The term $\langle\sigma v\rangle$ is the product of the reaction cross section $\sigma(E)$ and the relative velocity v averaged over the Maxwellian velocity distribution at temperature T. Knowledge of the radiative capture cross section $\sigma(E)$ at low energies is thus essential for an accurate description of the stellar environments where hydrogen burning through the β-limited CNO cycle can occur.

II. EXPERIMENTAL CONSIDERATIONS

A direct measurement of the ^{13}N(p,γ) cross section requires an intense radioactive ^{13}N beam. Efforts to obtain such beams are in progress at various laboratories around the world, for example, at Lawrence Livermore National Laboratory,[8] at TRIUMF,[9] and at Louvain-la-Neuve.[10] However, due to problems of low efficiency for producing the ^{13}N beam and with backgrounds in the beam it is not clear that any of these projects will yield a measurement

of Γ_γ in the near future.

An indirect determination of the $^{13}N(p,\gamma)^{14}O$ cross section can be made using a model for the low-energy reaction mechanism. The "hot" CNO cycle operates for temperatures $T \leq 10^9$ K,[5] which corresponds to $E \sim 100$ keV. In this energy range, the $^{13}N(p,\gamma)^{14}O$ reaction proceeds primarily via $E1$ transitions from $\ell = 0$ scattering states in $^{13}N+p$ to the 0^+ ground state in ^{14}O. The cross section will be dominated by the E_R=545 keV s-wave resonance corresponding to the 1^-, 5.17 MeV first excited state in ^{14}O, and should be well described by a single-level Breit-Wigner expression (see, for example, Ref. 11 and references therein), the input parameters of which can be measured using familiar nuclear spectroscopy techniques.[12]

The reliability of this indirect method for determining the low-energy $^{13}N(p,\gamma)$ cross section is illustrated by the very similar case of the $^{12}C(p,\gamma)^{13}N$ reaction, where the cross section has been measured for $E_p \geq 150$ keV.[13,14] The low-energy cross section is dominated by the E_R=422 keV, $\ell = 0$ resonance corresponding to the $\frac{1}{2}^+$, 2.37 MeV first excited state of ^{13}N. This cross section can be calculated using a single-level Breit-Wigner expression,[15] given the resonance energy E_R, proton width Γ_p, and gamma width Γ_γ of the $\frac{1}{2}^+$, 2.37 MeV level. A theoretical calculation using only these empirical parameters successfully describes the data over many orders of magnitude,[7] and demonstrates the validity of such an indirect determination of $\sigma(E)$.

To calculate the low-energy $^{13}N(p,\gamma)$ cross section, one needs E_R, Γ_p, and Γ_γ of the 1^-, 5.17 MeV level in ^{14}O. The resonance energy, $E_R = 545 \pm 10$ keV,[16] and total width $\Gamma = \Gamma_p + \Gamma_\gamma = 38.1 \pm 1.8$ keV (Ref. 17) have been determined. Since the expected value for Γ_γ is of the order of a few eV, we find $\Gamma_p = 38.1 \pm 1.8$ keV. On the other hand, only an upper limit of 17 eV exists for Γ_γ.[18] An experimental determination of Γ_γ for the first excited state in ^{14}O is therefore necessary for a reliable computation of the radiative proton capture cross section on ^{13}N at energies of astrophysical importance.

The $B(E1)$ of the $1^- \rightarrow 0^+$ transition in ^{14}O can be estimated from the observed $B(E1)$ for the $\frac{1}{2}^+ \rightarrow \frac{1}{2}^-$ transition in ^{13}N. In the single-particle picture, the transitions from the first excited states in ^{13}N and ^{14}O are both $2s_{1/2} \rightarrow 1p_{1/2}$ proton transitions. [The single-particle estimate for the ^{13}N transition is $B(E1)_{\text{s.p.}} = 0.14$ Weisskopf units (W.u.),[19] in very good agreement with the experimental value $B(E1)_{\text{exp}} = 0.13 \pm 0.01$ W.u. (Ref. 16).] Accounting for the difference in effective charges, this model predicts $B(E1)_{\text{s.p.}} = 0.075$ W.u., or $\Gamma_\gamma = 4.1$ eV for the $1^- \rightarrow 0^+$ transition in ^{14}O.

A slightly more elaborate prediction is given by the Zucker-Buck-McGrory (ZBM) model.[20] In this model, ^{13}N and ^{14}O are treated as a ^{12}C core with one or two protons in the $1p_{1/2}$, $2s_{1/2}$, or $1d_{5/2}$ orbits. The ZBM model and the single-particle model give the same description of the ground state and first excited state in ^{13}N and of the first excited state in ^{14}O. The ZBM prediction for the strength of the $1^- \rightarrow 0^+$ $E1$ transition in ^{14}O is $B(E1)_{\text{ZBM}} = 0.086$ W.u., or $\Gamma_\gamma = 4.7$ eV.[19] The 10% enhancement of $B(E1)_{\text{ZBM}}$ with respect to the single-particle model prediction is due to a 2.5% contribution of the $(2s_{1/2})^2$ configuration to the ground state of ^{14}O.

More elaborate estimates of the proton width Γ_p and the gamma width Γ_γ of the first excited state in ^{14}O are also available. The five more recent published calculations predict values for Γ_γ of 2.44 eV,[21] 1.9 eV,[22] 1.2 eV,[23] 1.6 eV,[11] and 4.1 eV.[24] These predicted values differ by as much as a factor of 3. The calculations use different methods, and there is *a priori* no reason to prefer any one of them. In fact, due to the inherent difficulty in estimating $E1$ transition strengths, the spread in the predicted values does not necessarily reflect the accuracy of the calculations. Parity changing processes, such as $E1$ transitions, are especially sensitive to small $2\hbar\omega$ components in the wave function of the positive parity state. These $2\hbar\omega$ components, which are difficult to calculate reliably since they involve the determination of numerous two-particle matrix elements, can have a large impact on the transition strength. In the particular case of the $1^- \rightarrow 0^+$ transition in ^{14}O, the most important contribution to the $E1$ matrix element comes from the overlap of the $2s_{1/2}$ and $1p_{1/2}$ proton wave functions. Because the $2s_{1/2}$ radial wave function has one node while the $1p_{1/2}$ has none, the radial integral is small. The $E1$ matrix element is therefore very sensitive to small admixtures of other configurations into the 1^- and 0^+ wave functions. The real value of Γ_γ could easily lie outside the predicted range; the only way to determine reliably the low-energy $^{13}N(p,\gamma)^{14}O$ cross section is to measure Γ_γ.

Because of the difficulty of measuring Γ_γ of an unbound level, it is worth considering alternatives to this measurement. The γ width of ^{14}O(5.17 MeV) could be inferred, at least in principle, from a measurement of the lifetime of the bound isospin analog state in ^{14}C. In the long wavelength limit, the $B(E1)$ values of transitions between analog levels in mirror nuclei should be identical.[25] A measurement of the width of the 6.09 MeV, 1^- level in ^{14}C, for example, in an electron scattering experiment, could then be used to infer Γ_γ of the analog transition in ^{14}O. Of course this method relies strongly on the assumption of isospin symmetry, and evidence for sizable violation of this symmetry would make the approach useless. Unfortunately, significant isospin symmetry violation occurs in the closely related $E1$ decays of the first excited states of ^{13}C and ^{13}N (all these decays are predominantly $2s_{1/2} \rightarrow 1p_{1/2}$ transitions); these should have equal strengths if isospin symmetry were exact. However, the measured $B(E1)$ in ^{13}N is roughly 3 times stronger than that in ^{13}C.[25,26] Although there is a considerable shift in the energies of these levels due to differences in the external radial wave functions,[27] these differences in the radial wave functions do not explain the $E1$ asymmetry.[26] The asymmetry is probably due to charge-dependent configuration mixing.[26,28] These con-

siderations rule out the measurement in ^{14}C as a possible approach to determine Γ_γ of the first excited state in ^{14}O.

On the other hand, it is possible (albeit difficult) to determine Γ_γ by measuring the γ-ray branching ratio Γ_γ/Γ of the unbound 5.17 MeV state in ^{14}O. The gamma width can then be extracted by combining the measured branching ratio with the known total width of this state. We followed this approach, producing ^{14}O(5.17 MeV) with the ^{12}C(^{3}He,$n\gamma$) reaction, and measuring Γ_γ/Γ by detecting coincidences between n_1 neutrons populating the ^{14}O state and 5.17 MeV γ-rays from its decay. The theoretical estimates for Γ_γ mentioned above correspond to Γ_γ/Γ in the range $(3.1\text{–}10.8)\times10^{-5}$. Such a small γ-decay probability indicated that maximizing the detection efficiency and minimizing the backgrounds would be crucial issues for our experiment.

III. EXPERIMENTAL SETUP

A. Beam

This experiment used beams from the University of Washington FN Tandem Van de Graaff accelerator. The n-γ coincidence yield was measured using a continuous ^{3}He beam, and taking time-of-flight (TOF) spectra between the neutron and the γ-ray detectors. The singles yield of neutrons populating the first excited state in ^{14}O was obtained using a pulsed ^{3}He beam and measuring the TOF between the neutron detector and the radio frequency (rf) signal from the beam buncher.

The optimum bombarding energy for our experiment was determined by a compromise between a large cross section for n_1 and a low γ-ray background: our figure of merit was Y_{n_1}/Y_γ, where Y_{n_1} is the yield of neutrons populating the first excited state in ^{14}O and Y_γ is the area of the prompt γ-ray peak in the singles neutron TOF spectrum. We scanned the region from 9.2 to 9.7 MeV taking singles neutron TOF spectra every 100 keV. The γ-ray yield remained flat within 10%, while the n_1 yield peaked in the region 9.3–9.4 MeV, producing a maximum in our figure of merit at 9.35 MeV. At this energy, zero degree neutrons populating the ground state and the first excited state in ^{14}O had energies of 7.75 and 1.93 MeV.

At our beam energy of $E_{^3\mathrm{He}} = 9.35$ MeV, only seven ^{3}He+^{12}C reaction channels are open, including the one of interest, ^{12}C(^{3}He,$n\gamma$). Taking into account the Coulomb barrier, ^{12}C(^{3}He,p)^{14}N is the only channel likely to produce γ rays above 4.5 MeV. The relatively low yield of high-energy γ rays encouraged us to attempt a simple measurement of Γ_γ/Γ by detecting γ rays rather than the more customary technique of detecting the recoiling heavy nucleus.

B. Detectors

Figure 1 shows a top view of the scattering chamber and detector arrangement. Gamma rays were detected in two 12.7 cm in diameter by 15.2 cm long NaI detectors placed on opposite sides of the scattering chamber at 90 deg with respect to the beam direction. This gave a high γ-ray detection efficiency: each detector subtended a solid angle that ranged from 25 ± 1 % (run 2) to 31 ± 1 % (run 1) of 4π. The high-voltage power supplies for the NaI photomultipliers were driven by gain stabilizers locked on the 511 keV line; this maintained a constant γ-ray energy calibration throughout a run, with a measured gain shift of $\leq$1% at 5.1 MeV. The ^{3}He beam stopping in the target backings produced an intense low-energy γ-ray yield ($E_\gamma \leq 300$ keV). A 1 mm thick sheet of lead placed in front of the NaI detectors attenuated these low-energy γ rays. Larger amounts of lead, set up as shielding around the collimators and between the γ-ray and neutron counters, reduced random and γ-γ coincidences.

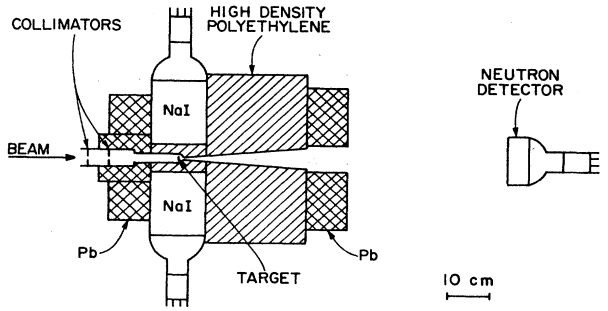

FIG. 1. Top view of the target chamber and detector arrangement.

Neutrons were detected in a 12.7 cm diam by 5.1 cm thick cell of BC-501 liquid scintillator, having excellent pulse shape discrimination properties. The detector was placed 82 cm from the target at $\theta_n = 0°$, where the differential cross section for ^{12}C(^{3}He,n_1) is maximum.[29] The pulse shape discrimination was performed by a Canberra 2160A pulse shape discriminator (PSD).

The target chamber, a 2.54 cm diam Ta-lined Pyrex tee, accomodated two targets in a Ta target ladder. The beam stopped in the target backings, which were either 0.25 mm Ta or 0.5 mm Au substrates. All vacuum seals were made with Viton O-rings. A beamline base vacuum of 5×10^{-7} torr was achieved by a cryo pump and a liquid-nitrogen-cooled trap located upstream from the target. The measured contaminant build-up for a 100 h long run with 10 nA of 9.35 MeV ^{3}He beam on target was $\leq$5 μg/cm^2 of natural carbon and $\leq$0.005 μg/cm^2 of nitrogen.

Two Ta collimators constrained the beam to a localized spot on the target. This helped to maintain a constant geometrical detection efficiency, and made the coincidence-to-singles yield ratio less sensitive to target thickness nonuniformities. We checked our sensitivity to the motion of the beam position on the target by placing single channel analyzers (SCA's) with a 3.5 MeV threshold on the γ-ray energy signals. Because these SCA's scaled only the counts produced by the beam hitting the target, and not by radioactivity or by reactions on the backing, their counts were sensitive to fluctuations in the

beam position on the target. The ratio of SCA counts to the beam charge differed by less than 2.5% between the $^{12}C+^{3}He$ singles and coincidence runs.

The $^{12}C(^{3}He,n)^{14}O$ reaction produced a subtle background of its own: neutrons populating the ground state in ^{14}O could inelastically scatter in the NaI detectors and then be detected in the neutron counter, producing a "n-γ" coincidence background that corresponded to a spurious γ-ray "branching ratio" of $(1.8 \pm 0.1) \times 10^{-3}$, about 40 times larger than the expected real value. This background was reduced to an acceptable level by installing a high-density polyethylene neutron shield between the NaI detectors and the neutron counter. The target was almost entirely surrounded with attenuating material; only the forward cone subtended by the neutron detector was unobstructed. With the NaI detectors at 3.65 cm from the target, neutrons that scattered in the NaI detectors had to pass through at least 14 cm of polyethylene before reaching the neutron detector. With the shield installed, the background "branching ratio" was $(2.2 \pm 0.6) \times 10^{-4}$, a factor of 8 below the unshielded result.

C. Targets

We investigated our sensitivity to target contaminants by taking ($^{3}He,n\gamma$) coincidence data on natural N, O, NaCl, Al, Si, Fe and enriched ^{13}C targets. All targets, except for O and Si, showed a considerable yield of $\approx$2 MeV neutrons in coincidence with 5.0–5.3 MeV γ rays. For example, the coincidence yield from 0.05 $\mu g/cm^2$ of N, 0.3 $\mu g/cm^2$ of ^{13}C, or 0.003 $\mu g/cm^2$ of Al, would be enough to give a false coincidence signal equal to the expected real signal from $^{12}C(^{3}He,n_1\gamma)^{14}O$. The best evaporated ^{12}C target that we could obtain[30] contained 0.14 $\mu g/cm^2$ of ^{14}N, enough to yield a false "branching ratio" of 1.3×10^{-4}, more than twice the expected real branching ratio. It also contained traces of NaCl and Si, plus other unidentified contaminants. Since it did not seem practical to obtain a significantly better evaporated target, we made our ^{12}C target by implanting $\approx$400 $\mu g/cm^2$ of ^{12}C into a 99.9985% pure Au backing,[31] using a sputter ion source. Special attention was paid to minimizing contamination of the target throughout the fabrication procedure; details can be found in Ref. 32. By continuously sweeping the ^{12}C beam across the Au substrate, we obtained a target uniform to within 10% over a 0.32 cm diam central area; this was adequate since the beam spot on the target was determined by a 0.27 cm diam defining collimator.

The ^{12}C target was tested for contaminants using a Ge(Li) detector to detect γ rays emitted when the target was bombarded with 3.9 MeV protons (at this energy there is no yield from the first excited state in ^{12}C at 4.44 MeV, making it easier to see weak γ-ray lines from small amounts of contaminants). Spectra accumulated during bombardment of the front and back of the targets were very similar. The only excess on the carbon side was $\leq$0.1 $\mu g/cm^2$ of ^{13}C (at least 3 times less than the amount required to give a coincidence yield comparable to that expected from ^{14}O decays) and $\leq$0.01 $\mu g/cm^2$ of ^{14}N (14 times less than in our best evaporated target). Because this test was carried out after two 100 h long data taking runs, during which the target had been irradiated with an average current of 8 nA, part or all of the ^{13}C and ^{14}N found in the ^{12}C target could have been deposited during the runs.

D. Electronics

The signal-processing electronics had three main sections: fast electronics for timing, slow electronics for pulse height information, and pulse shape discrimination on the neutron detector. Using a ^{22}Na source, typical time resolution of the prompt γ-ray peak in the TOF spectra between the neutron counter and each of the NaI detectors was 5.5 ns. The NaI energy signals were fed into special 50 Ω input impedance charge-sensitive preamplifiers that drove Ortec 460 delay line amplifiers with 1 μs clipping lines. The short duration of the output pulses helped minimize pileup effects.

Our data acquisition system consisted of a Digital Equipment Corporation DEC PDP 11/60 computer with a CAMAC-based experiment interface. Six parameters of each event were recorded by Tracor Northern TN-1213 Analog-to-digital converters (ADC's): pulse height in the neutron detector, PSD signal, γ-ray energy in each NaI, and TOF between the neutron counter and each of the NaI detectors. The master trigger was the logic OR of the valid conversion output (true stop) of each NaI time-to-amplitude converter (TAC). Ten scalers counted the beam charge on the target, the beam charge on the collimators, the constant fraction discriminator (CFD) output pulses for the three detectors, the nuclear magnetic resonance (NMR) frequency that determines the beam energy, the time elapsed during the run, the master trigger for data collection, and the two SCA's on the γ-ray energy signals.

The only change needed to switch from dc beam coincidence data to pulsed beam singles data was to replace the stop signals in the NaI TAC's by the rf signal derived from the low-energy buncher. Both TAC's then reflected the neutron TOF between the target and the neutron detector. No other changes were made in the electronics or data taking procedure so that we could be assured of a consistent neutron detection efficiency for the singles and coincidence runs.

The data acquisition live fraction, defined as the ratio of events written on tape to scaled master triggers, was a strong function of the event rate. In coincidence mode, the rate was typically 60 events/s, and the corresponding live fraction was 97.7%. During the singles runs, the rate could get as high as 400 events/s, with a live fraction of 85.5%. From these results we estimated the dead time of the data acquisition system to be $\approx 4 \times 10^{-4}$ s. The measured reaction yields were corrected for this dead time.

IV. DATA ANALYSIS

The ^{14}O(5.17 MeV) γ-ray branching ratio Γ_γ/Γ is obtained from the expression

$$\frac{\Gamma_\gamma}{\Gamma} = \frac{Y^C_{n_1}}{Y^S_{n_1} \times \eta \times \widetilde{W}(\theta)} ,$$

where $Y^C_{n_1}$ is the n-γ coincidence yield, $Y^S_{n_1}$ is the n_1 singles yield, η is the efficiency for detecting 5.17 MeV γ rays, and $\widetilde{W}(\theta)$ is the n-γ angular correlation. We had two week-long data taking runs, and a third week-long run to test for systematic errors. In each run we measured all the ingredients required to determine Γ_γ/Γ: the n_1 singles yield, the n_1 yield in coincidence with 5.17 MeV γ rays, and the NaI detector efficiencies at 5.17 MeV.

A. ^{12}C(^{3}He,n) singles yield

A typical ^{12}C(^{3}He,n) singles TOF spectrum, sorted from our event data without any constraints, is shown in Fig. 2. A two-dimensional (2D) spectrum of pulse height in the neutron detector against the PSD signal, gated on the n_1 group in the TOF spectrum, is shown in Fig. 3. Such gated spectra were used to choose the 2D cut corresponding to 1.93 MeV n_1 neutrons in the liquid scintillator.

The singles neutron yield, $Y^S_{n_1}$, was obtained by sorting the TOF data on the 2D n_1 constraint. A typical result is shown in Fig. 4. The effect of this 2D cut can be readily seen: the prompt γ-ray peak in this spectrum is suppressed by a factor of $\approx$6000 compared to Fig. 2. The yield of n_0 neutrons populating the ^{14}O ground state is also suppressed; the cut on the neutron detector pulse height preserved most of the n_1 neutrons, but included only a small fraction of the n_0 group.

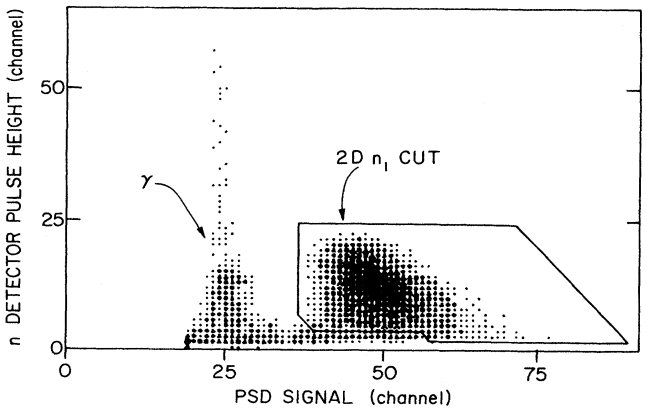

FIG. 3. Pulse height in the neutron detector vs PSD signal for ^{12}C(^{3}He,n) pulsed-beam singles data gated on the flight time for the n_1 group. The 2D n_1 cut used in the analysis of the singles and coincidence data is indicated.

B. ^{12}C(^{3}He,$n\gamma$) coincidence yield

In each week-long run we accumulated 100 h of ^{12}C(^{3}He,$n\gamma$) coincidence data. The beam current was limited to $\approx$ 10 nA by the count rate in the NaI detectors. We maintained the NaI CFD rates (thresholds at $E_\gamma \approx 300$ keV) at 75 kHz, which corresponded to a rate of 32 kHz for $E_\gamma > 511$ keV. At these rates, the pileup in the NaI detectors was estimated to be less than 15%.

Our analysis of the coincidence data was based on empirical line shapes of 1.93 MeV neutrons in the TOF spectrum and of 5.11 MeV γ rays in the NaI detectors. The neutron line shape (see Fig. 5) was measured using the ^{16}O(^{3}He,$n\gamma$)^{18}Ne reaction at

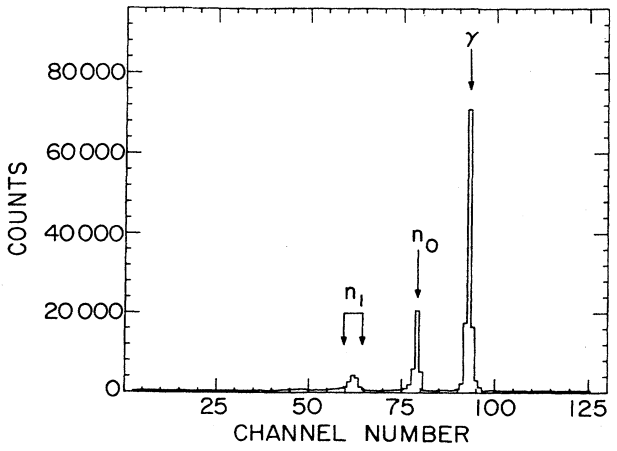

FIG. 2. Neutron TOF singles spectrum for ^{12}C(^{3}He,n), sorted with no constraints.

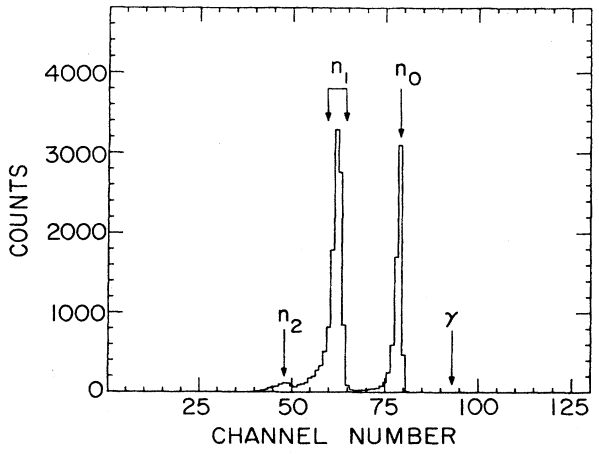

FIG. 4. Neutron singles TOF spectrum for ^{12}C+^{3}He, sorted with the 2D n_1 constraint. The weak n_2 group is now noticeable. The window used to determine the singles n_1 yield is indicated.

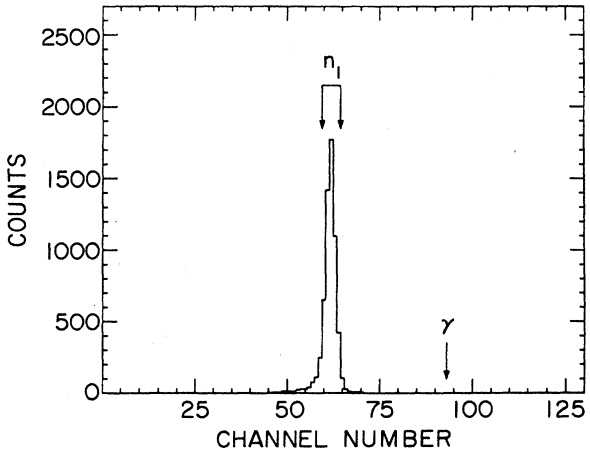

FIG. 5. Coincidence TOF line shape for a 1.93 MeV neutron, measured using the ^{16}O(^{3}He,$n_1\gamma$)^{18}Ne reaction. This spectrum was obtained by sorting the data on the 2D neutron constraint and a 1.89 MeV γ-ray window in the NaI detector.

$E_{^3\mathrm{He}}$= 7.62 MeV. At this bombarding energy the n_1 group from ^{16}O(^{3}He,n) had the same flight time as the n_1 group from ^{12}C(^{3}He,n) at 9.35 MeV. The line shape for a 5.11 MeV γ ray (see Fig. 6) was measured using the ^{11}B(^{4}He,$n\gamma$)^{14}N(5.11 MeV) reaction at $E_{^4\mathrm{He}} = 7.5$ MeV. This line shape was then shifted to match the expected location of a 5.17 MeV γ ray. Because the first-escape peak accounts for a considerable fraction of the integrated line shape, we chose a "wide cut" that included the photo and first-escape peaks. The alternative "photopeak cut" shown in Fig. 6 was used to test the sensitivity of our results to the choice of cuts (see below).

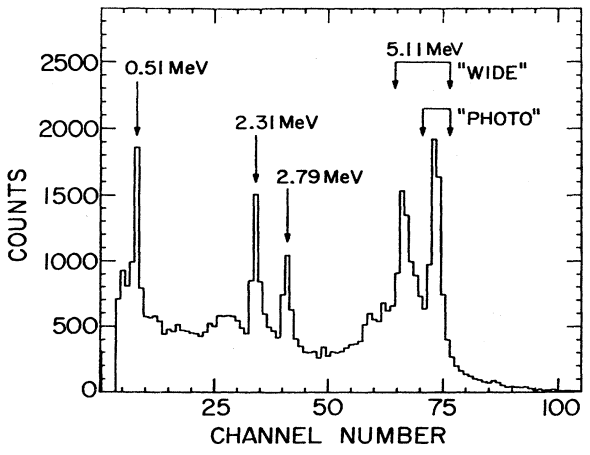

FIG. 6. NaI line shape for a 5.11 MeV γ ray from ^{11}B(^{4}He,$n_4\gamma$)^{14}N. The lines at 2.79 and 2.31 MeV are produced in a weaker cascade decay of the 5.11 MeV state. The "wide" and "photopeak" cuts are shown.

The ^{12}C(^{3}He,$n\gamma$) coincidence data were analyzed by generating 2D E_γ vs TOF spectra for each NaI detector; all events had to satisfy the same 2D n_1 constraint used in the ^{12}C(^{3}He,n) singles analysis. These spectra were then projected onto the E_γ and TOF axes using 1.93 MeV neutron and 5.17 MeV γ-ray cuts based on the measured line shapes (see Figs. 5 and 6). The projection onto the vertical axis yielded the spectrum of γ rays in coincidence with 1.93 MeV neutrons, while the projection onto the horizontal axis gave the neutron TOF spectrum in coincidence with 5.17 MeV γ rays. Four sets of one-dimensional (1D) E_γ and TOF spectra, one for each NaI detector for each run, were analyzed to obtain the yield, $Y^C_{n_1}$, of n_1 neutrons in coincidence with 5.17 MeV γ rays. We simultaneously fitted the four data sets with a function having four components: accidental coincidences, target backing background, neutron scattering background, and n-γ coincidences from the γ decay of ^{14}O(5.17 MeV). The contributions due to the randoms and the target backing were fixed as described below. The other two contributions were determined by adjusting the nine free parameters of the fitting function: eight parameters describing the neutron scattering background (two for each set of coincidence data), the ninth parameter was the branching ratio Γ_γ/Γ. The best values for these parameters were determined by a χ^2 minimizer code.

(i) *Accidental coincidences*: The γ-ray spectra of random coincidences were obtained by sorting the ^{12}C(^{3}He,$n\gamma$) data with a window in the flat region of the neutron TOF spectrum (long flight times). Since there were no time correlated events between the neutron and γ-ray detectors in this chosen random TOF window, the shape of the NaI accidental coincidences did not depend on whether the neutron detector was triggered by a γ ray or a neutron. To get the best possible statistics, we therefore did not use the 2D n_1 constraint in obtaining the γ-ray spectra of accidental coincidences.

Figure 7 shows a spectrum of accidentals in the NaI detectors. The structure in the spectrum was due to γ

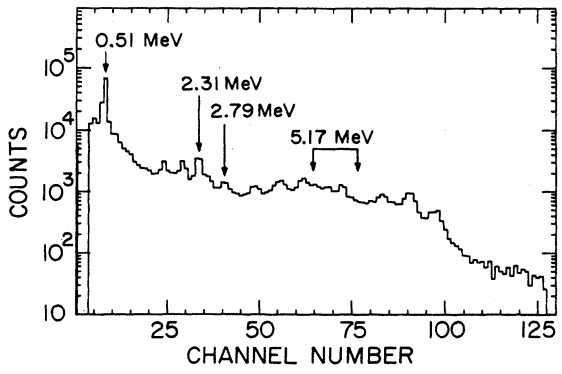

FIG. 7. Accidental coincidences in the gamma detectors. The window indicates the 5.17 MeV cut used in the analysis of the coincidence data. The structure in the spectrum is due to γ-ray decays in ^{11}C, ^{12}C, and ^{14}N.

rays produced in the ^{12}C(^{3}He,^{4}He)^{11}C, ^{12}C(^{3}He,p)^{14}N, and ^{12}C(^{3}He,^{3}He$'$)^{12}C* reactions. The peak inside the window at 5.17 MeV corresponded to the decay of the 5.11 MeV state of ^{14}N; γ rays at 2.31 and 2.79 MeV from a weaker branch of this decay can also be seen. These three γ rays were also observed in the NaI line shape measurement, Fig. 6. This allowed us to monitor the long-term gain stability of the detectors and verify that our γ-ray energy calibrations were correct. We also obtained a random NaI spectrum gated on the 2D n_1 constraint. The ratio of the counts in the 5.17 MeV window in this spectrum and in the higher statistics random spectrum was used as the scaling factor for the random contribution to the γ-ray energy fitting function.

The random counts in the TOF spectrum should be distributed as

$$N(t) = \text{const} \times e^{-t/\tau} ,$$

where $\tau=(R_{\text{stop}})^{-1}$ is determined by the rate of TAC stop pulses. Since the stop pulse rate was 75 kHz, the exponential decrease of the random background over the 160 ns spanned by the TOF spectra is $\approx$ 1%. We neglected this small correction and assumed a flat random distribution.

(ii) *Target backing background*: We determined the contribution of the Au backing by measuring the n-γ coincidence yield from the back of the target. The average beam current during these runs was 180 nA, and the CFD rate was 25 kHz. These data were sorted in the same way as the ^{12}C data. The γ-ray spectrum in coincidence with 1.93 MeV neutrons showed peaks at 1.89 MeV and 1.49 MeV; these γ rays were produced in the ^{16}O(^{3}He,$n\gamma$)^{18}Ne reaction on residual oxygen in the Au substrate. The target backing contribution to the neutron TOF fitting function was a smooth curve that contained the same information as the measured backing coincidence TOF spectrum. When multiplied by the ratio of beam charges for the ^{12}C and backing coincidence runs, these NaI and TOF spectra became the target backing contribution to the coincidence fitting function.

(iii) *Neutron scattering background*: The shapes of the neutron scattering background contributions to the γ-ray and neutron TOF coincidence spectra were determined from data taken in a third week-long run. In this run we removed the high-density polyethylene shield, and ran with one detector in the geometry used in run 1, and the other at the distance from the target used in run 2. The NaI spectra from scattered neutrons were well described by decaying exponentials. The shape of the background in the TOF spectra was determined by the following procedure. We first obtained a TOF spectrum of neutrons in coincidence with 2.8 MeV γ rays. The observed yield, once the contribution from the target backing had been subtracted, was assumed to be due entirely to the neutron scattering background. We found a smooth curve that described the data, and then allowed the width and centroid of this curve to vary in order to fit the observed TOF yield in coincidence with γ rays at 2, 3.6, 4.1, 4.6, 5.17, 5.6, and 6.1 MeV. The agreement between the data and the fit was very good at all these energies, see, for example, Fig. 8. These fits to the unshielded data provided us with the neutron scattering contribution to the fitting function for the analysis of the shielded ^{12}C(^{3}He,$n\gamma$) coincidence TOF spectra.

(iv) *Gamma-ray decays in* ^{14}O: The n-γ coincidences from decays in ^{14}O were described by the 5.17 MeV line shape in the NaI detectors, Fig. 6, and by the 1.93 MeV neutron line shape in the TOF spectra, Fig. 5. The scaling factor for the line shapes was proportional to the γ-ray branching ratio Γ_γ/Γ, which was one of the nine free parameters of the fitting function. The NaI detector efficiency at 5.17 MeV (see Sec. IV C) and the angular correlation $\widetilde{W}(\theta)$ (see Sec. IV D) were used in the computation of Γ_γ/Γ.

With these four components, we constructed a fitting function that satisfied the following constraint: each component contributed the same number of counts to the 5.17 MeV window in the coincidence NaI spectrum, and to the 1.93 MeV window in the corresponding neutron TOF coincidence spectrum. The fact that the two spectra were orthogonal projections of the same 2D data was thus taken into account. The error in the γ-ray branching ratio Γ_γ/Γ was determined by the amount by which its associated parameter in the fitting function had to change to increase the minimum χ^2 by one, including the effect of correlations with the other eight free parameters of the fitting function. This amount was multiplied by $(\chi^2/\nu)^{1/2}$ (ν =number of degrees of freedom) if χ^2 was greater than ν. The uncertainties in the n_1 singles

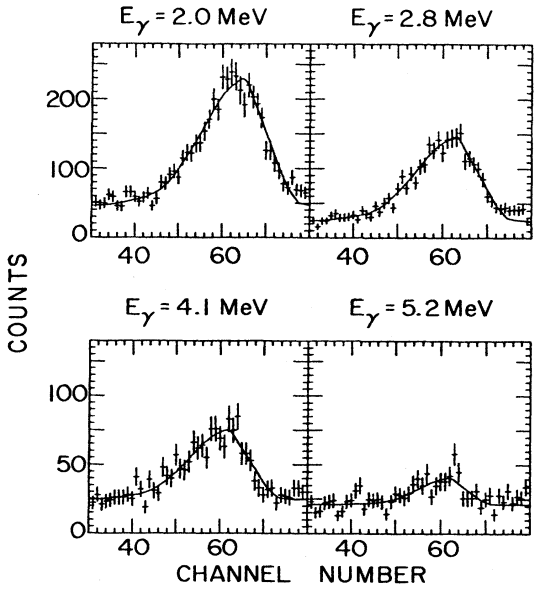

FIG. 8. Neutron scattering background contribution to the TOF coincidences, for the geometry of Run 1. The smooth curve was determined by the data in coincidence with 2.8 MeV γ rays.

yield, the n-γ angular correlation, and the γ-ray detection efficiency were then added in quadrature.

We simultaneously analyzed our four sets of $^{12}C(^3He,n\gamma)^{14}O$ coincidence spectra, fitting the data only in the region where we had useful information on the line shapes, for example, from channel 55 to 78 in the NaI spectrum (Fig. 6) and from channel 43 to 67 in the TOF spectrum (Fig. 5). Figure 9 shows the resulting fit to one set of the data. The γ-ray branching ratio obtained from this simultaneous fit to all our data is $\Gamma_\gamma/\Gamma = (8.5 \pm 3.5) \times 10^{-5}$, with $\chi^2/\nu = 1.106$ for $\nu = 186$, $P_{\chi^2} = 16.4\%$. Figure 10 shows the combined neutron TOF coincidence data for $^{12}C(^3He,n\gamma)$ and the best fit. The breakdown of the fitting function into its four components is shown as well.

This γ-ray branching ratio must be corrected for small backgrounds from ^{13}C and ^{14}N contaminants in the target. The amounts of these contaminants were measured by scattering 3.9 MeV protons on the ^{12}C target and on ^{13}C and natural melamine targets as described in Sec. III C. We carried out this measurement twice, after the second and third week-long runs, and found out that the contaminants had built up linearly with the running time. We measured the n-γ coincidence yield from ^3He on the same ^{13}C and natural melamine targets, and subtracted their contribution to the ^{12}C coincidence yield. This correction reduced the ^{14}O γ-ray branching ratio to $\Gamma_\gamma/\Gamma = (7.2 \pm 3.5) \times 10^{-5}$.

The combined neutron TOF data (Fig. 10, top panel) showed an excess of fast neutrons in the region $E_n \approx 2.6$–13 MeV (channels 68–83), presumably due to an unidentified target contaminant. The combined $(^3He,n\gamma)$ TOF data on the back of the target (Fig. 10, third panel) did not show enough yield of fast neutrons to account for the observed excess on the target front. Therefore, any contaminant present in equal amounts in the front and back of the ^{12}C target could not be the cause of the background. This consideration ruled out NaCl, Al, Si, Ni, and Fe, which had been identified in the $(p,p'\gamma)$ Ge(Li) spectra discussed in Sec. III C. Oxygen was also discarded since it had been clearly identified in the $(^3He,n\gamma)$ coincidence data on both the front and the back of the target, but the amount of ^{16}O on the target was only 60–70% of the amount in the backing (presumably ion implantation drove some of the oxygen from the gold substrate). Nitrogen and ^{13}C were also excluded since $(^3He,n\gamma)$ coincidence data taken on a natural melamine target and on an enriched ^{13}C target did not show the fast n-γ background. Another possibility was that a small amount of ^{11}BH could have been implanted in the target; the $^{11}B(^3He,n)$ reaction strongly populates the 6.88 MeV level in ^{13}N,[33] producing 12.4 MeV neutrons in coincidence with 4.44 MeV γ rays from the decay of the 6.88 MeV level to the first excited state in ^{12}C. In this case, we should have seen 4.44 MeV γ rays in coin-

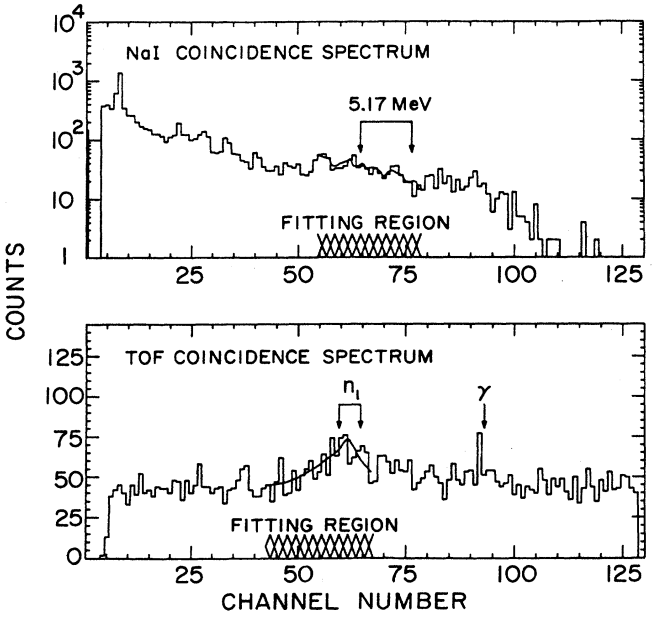

FIG. 9. Fit to the $^{12}C(^3He,n\gamma)$ coincidence spectra. The 5.17 MeV γ ray and 1.93 MeV neutron windows used in the analysis of the data, and the fitting regions, are indicated.

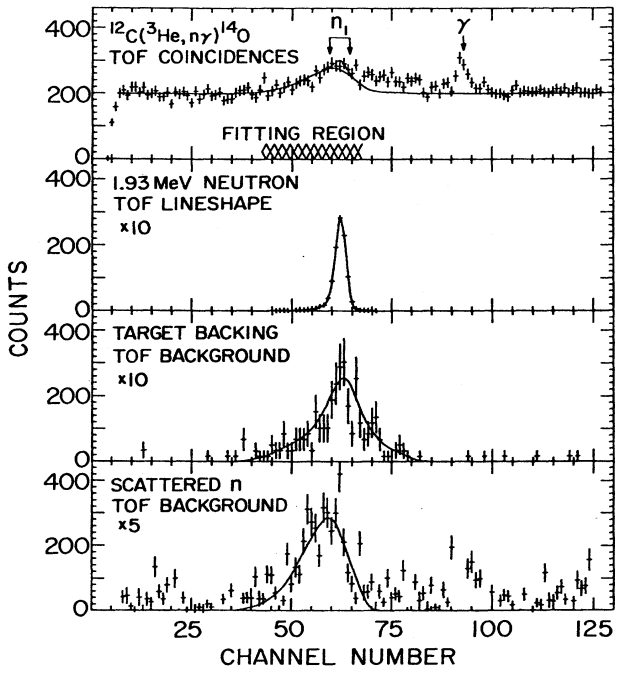

FIG. 10. Fit to the combined neutron TOF coincidence data. The top panel is the summed TOF data from $^{12}C+^3He$; the lower solid curve is the sum of the the backing, randoms, and neutron scattering background components of the fit; the upper curve includes the ^{14}O decays. The other panels show the ingredients of the fit; the points are actual data, while the curves are the components of the fitting function. The 1.93 MeV window and the fitting region are indicated.

cidence with the fast neutrons; we did not and therefore discarded the ^{11}B hypothesis. Since the spectrum of γ rays in coincidence with the fast neutrons did not show any clear γ-ray lines that could identify the contaminant, the background remains unexplained. The contribution of this background to the n-γ coincidence spectra would have to resemble a 1.93 MeV neutron in coincidence with a 5.17 MeV γ ray in order to have a significant impact on our results. Under this light, a very conservative approach would be to interpret our result as a one standard deviation upper limit for the γ-ray branching ratio, $\Gamma_\gamma/\Gamma < 1.07 \times 10^{-4}$.

We also analyzed our coincidence data using only the 1D neutron TOF spectrum that resulted from combining our four sets of data (top panel in Fig. 10). We fitted this 1D spectrum with a two-parameter fitting function. The four components of this function corresponded identically to the components shown in Fig. 10; the accidental and backing contributions were fixed, while the amplitude of the neutron scattering background and the number of observed ^{14}O decays (i.e. 1.93 MeV neutron line shape) were allowed to vary. This analysis of the 1D neutron TOF data yielded $\Gamma_\gamma/\Gamma = (6.5 \pm 3.8) \times 10^{-5}$, with $\chi^2/\nu = 1.237$ for $\nu = 23$, $P_{\chi^2} = 21.0\%$. This 1D analysis agrees well with the result of the simultaneous analysis of both the γ-ray energy and neutron TOF spectra.

Next we repeated the 2D analysis of the γ-ray and neutron TOF coincidence spectra independently for each of our four sets of data. The statistical average of these four determinations of the branching ratio, $\Gamma_\gamma/\Gamma = (6.8 \pm 3.4) \times 10^{-5}$, agrees very well with the result from the simultaneous analysis of all the data. However, the standard deviation of these four determinations of Γ_γ/Γ was 1.7 times larger than the statistical error in our measurement. Since the probability that the four measurements would have this spread is only 2.2%, we checked our data for indications of systematic errors. A thorough examination showed no evidence of nonstatistical behaviour in our data, and we conclude that, albeit improbable, the spread in the four measurements of the branching ratio is a statistical occurrence. We then use the statistical error to quote our result for the γ-ray branching ratio, $\Gamma_\gamma/\Gamma = (7.2 \pm 3.5) \times 10^{-5}$.

We checked the sensitivity of our result to the choice of window width for the 5.17 MeV γ ray by repeating the analysis with the "photopeak" γ-ray cut shown in Fig. 6, and obtained $\Gamma_\gamma/\Gamma = (6.6 \pm 3.7) \times 10^{-5}$, with $\chi^2/\nu = 0.968$ for $\nu = 186$, $P_{\chi^2} = 60.3\%$, in very good agreement with the "wide" cut result. Finally, we analyzed the ^{12}C(^{3}He,$n\gamma$) coincidence data assuming that the n-γ coincidences occurred for energies other than $E_{n_1} = 1.93$ MeV and $E_\gamma = 5.17$ MeV. If the fitting function had been wrong, the χ^2 minimizer code could have found γ-decay strength regardless of the neutron and γ-ray energy. We first kept the neutron energy fixed at 1.93 MeV, and searched for coincidences with γ rays at 4.1, 4.6, 5.6, and 6.1 MeV. Conversely, we assumed a neutron energy of 1, 1.5, 2.5, and 3 MeV in coincidence with a 5.17 MeV γ ray. Lastly, we kept the sum of the neutron and γ-ray energies fixed to 1.93 MeV + 5.17 MeV = 7.1 MeV; this check tested the description of the neutron scattering background, since the observed energy was conserved in this process. The resulting branching ratios and their χ^2 probabilities are shown in Fig. 11. These tests indicated that n-γ coincidences in our ^{12}C(^{3}He,$n\gamma$)^{14}O data occurred with non-negligible probability only for $E_{n_1} = 1.93$ MeV *and* $E_\gamma = 5.17$ MeV. The positive results of these tests are an important source of confidence in our measured 2 standard deviation effect.

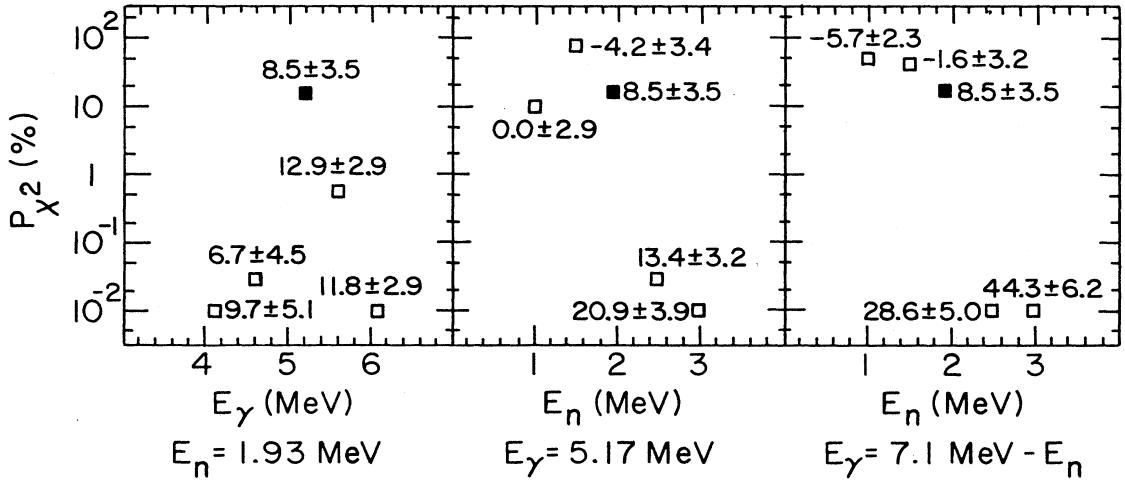

FIG. 11. Probability of the "best fit" χ^2 for different assumed γ-ray and neutron energies. The "best fit" branching ratio ($\times 10^5$) obtained by the fitting code is indicated at each point. The only statistically significant positive results occur for $E_n = 1.93$ MeV *and* $E_\gamma = 5.17$ MeV.

C. Gamma-ray detection efficiency

The γ-ray detection efficiency at several energies was found by populating levels with known γ-decay branching ratios in the ^{11}B(^{4}He,$n\gamma$)^{14}N ($E_{^4\mathrm{He}}$=7.5 MeV) and ^{16}O(^{3}He,$n\gamma$)^{18}Ne ($E_{^3\mathrm{He}}$=7.62 MeV) reactions. We determined the "photopeak" efficiencies [η_{photo} corresponds to the yield on a window centered on the photopeak with a width twice the photopeak full width at half maximum (FWHM)] at 1.64, 1.89, 2.31, 4.92, and 5.11 MeV, and the "wide" efficiencies (η_{wide} corresponds to a window wide enough to include the first escape peak) at 4.92 and 5.11 MeV, assuming isotropic n-γ angular correlations. This assumption is strictly true only for the 2.31 and 4.92 MeV γ rays emitted by J=0 states in ^{14}N. However isotropy was not a bad assumption for the other decays, since the large solid angle subtended by the NaI detectors attenuated the effects of any anisotropic correlation. The photopeak efficiency was also measured at 0.66, 1.26, and 1.27 MeV using calibrated radioactive sources of ^{137}Cs, ^{60}Co, and ^{22}Na. Figure 12 shows the measured "photopeak" and "wide" efficiencies of one NaI detector for run 1 along with the efficiencies predicted by the Monte Carlo code EGS4.[34] This code allows for the inclusion of the different media between the target and the γ-ray detectors, in a geometry that approximates the experimental setup. The Monte Carlo calculation reproduces the trend of the data reasonably well, in particular at the higher energies. (The overall ≈30% discrepancy at the lower energies is probably due to an approximate description of the complicated experimental geometry.) We used these Monte Carlo calculations to extrapolate the efficiency at 5.17 MeV from the measured values of η_{photo} and η_{wide} at the highest-energy isotropic γ ray in our calibration data (4.92 MeV), and obtained

$$\eta(5.17\ \mathrm{MeV}) = 0.97 \times \eta(4.92\ \mathrm{MeV})\ .$$

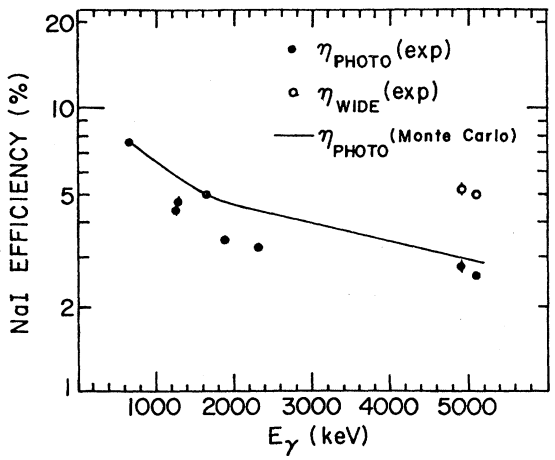

FIG. 12. Measured "photopeak" and "wide" efficiencies for detector NaI 1 in run 1 ($\Delta\Omega/4\pi = 0.31 \pm 0.01$). The solid line indicates results from a Monte Carlo calculation.

As expected, η_{wide} was roughly twice η_{photo} at 5.17 MeV. Since the background at this γ-ray energy in the ^{12}C(^{3}He,$n\gamma$) coincidence data was reasonably smooth, it was advantageous to use the "wide" γ-ray window: we included a significantly larger fraction of the real signal, while keeping the signal-to-noise ratio unchanged.

D. Angular correlation $\widetilde{W}(\theta)$

Because our circular neutron detector was placed at $\theta_n = 0°$ the apparatus for producing ^{14}O(5.17 MeV) was symmetric about the beam axis. Therefore, the n-γ angular correlation $W(\theta)$ is given by[35,36]

$$W(\theta) = \frac{1}{4\pi}[1 + a_2 P_2(\cos\theta)]\ ,$$

where θ is the angle between the photon and the symmetry axis, and a_2 is determined by the population of the magnetic substates of the decaying J=1 level.

The substate population depends on the ^{12}C(^{3}He,n) reaction mechanism. The most likely mechanism is direct single-step two-nucleon stripping, where the two protons are transferred in a J=0 state and the neutron is a spectator. Since the ^{12}C target has J=0, angular momentum conservation along the beam axis allows only M=0 substates of ^{14}O to be populated. This mechanism is consistent with the observed angular distribution of neutrons populating the 5.17 MeV state in ^{14}O; the excitation functions and angular distributions for ^{12}C(^{3}He,n)^{14}O(5.17 MeV) at $E_{^3\mathrm{He}}$= 10, 11, and 12 MeV are well described at forward angles ($\theta < 50°$) by a distorted-wave Born approximation (DWBA) calculation that assumes that the reaction proceeds by transferring two protons in a single step.[29] It is thus likely that the direct reaction mechanism is already dominant at $E_{^3\mathrm{He}}$ =9.35 MeV.

Studies of other dinucleon stripping reactions in light nuclei at similar bombarding energies also support the direct two-nucleon stripping reaction mechanism. Angular correlation measurements of decay protons in the ^{12}C(^{3}He,p)^{14}N reactions at $E_{^3\mathrm{He}}$ = 12 MeV indicate that T=1 unbound states in ^{14}N are populated essentially purely in the M=0 magnetic substate.[37,38] For example, the measured population parameter for the M=0 substate of the 8.91 MeV level was $P(0) = 0.99^{+0.01}_{-0.07}$, in excellent agreement with the direct reaction prediction, $P(0)$=1.[39] Similar confirmations of the direct reaction mechanism were found in angular correlation studies in ^{14}C($t,p\gamma$)^{16}C, E_t = 12 MeV,[40] and ^{10}Be($t,p\gamma$)^{12}Be, E_t = 12 MeV.[41] The measured population parameters in these cases agreed to within 15% or better with the direct reaction predictions.

Based on this evidence, we expect that $P(0)$=1 will be a very good approximation in our case. Therefore, the angular distribution of the $E1$ transition to the J=0 ground state is[42]

$$W(\theta) = \frac{3}{8\pi}\sin^2\theta$$

which corresponds to $a_2 = -1$. We assign a 10% error to a_2; this uncertainty is consistent with the measured values of the $M=0$ population parameter in similar cases.[37,40,41] The n-γ angular correlation corrected for the finite solid angles subtended by the γ-ray detectors[43] is

$$\widetilde{W}(\theta) = \frac{1}{4\pi}[1 + a_2 Q_2 P_2(\cos\theta)] .$$

The angular correlation attenuation coefficient for the photo plus first escape peaks, Q_2, was obtained from a Monte Carlo calculation.[44,45] The resulting angular correlations were

$$4\pi\widetilde{W}(\theta = 90°) = 1.30 \pm 0.08$$

for run 1 and

$$4\pi\widetilde{W}(\theta = 90°) = 1.35 \pm 0.08$$

for run 2.

V. ASTROPHYSICAL S FACTOR FOR THE ^{13}N(p,γ)^{14}O REACTION

Combining our measured γ-ray branching ratio for the 5.17 MeV state in ^{14}O, $\Gamma_\gamma/\Gamma = (7.2 \pm 3.5) \times 10^{-5}$, with the known total width $\Gamma = 38.1 \pm 1.8$ keV,[17] we obtain $\Gamma_\gamma = 2.7 \pm 1.3$ eV, which agrees with all five of the more elaborate theoretical estimates mentioned in Sec. II. Our measurement is in marginal agreement with a preliminary experimental result by Aguer *et al.*[46] who obtained $\Gamma_\gamma/\Gamma = (2\pm1)\times10^{-4}$ or $\Gamma_\gamma = 7.6\pm3.8$ eV. Wang *et al.*[47] reported a preliminary result using the ^{1}H(^{14}N,^{14}O)n reaction. They obtain

$$\Gamma_\gamma \times \frac{\sigma_{n_1}}{\sigma_{n_0}} = 1.38 \pm 0.66 \text{ eV}$$

from a ^{14}O(5.17 MeV) singles measurement, and

$$\Gamma_\gamma \times \frac{\sigma_{n_1}}{\sigma_{n_0}} = 0.97 \pm 0.31 \text{ eV}$$

from a γ-^{14}O(5.17 MeV) coincidence measurement, where σ_{n_0} and σ_{n_1} are the cross sections for populating the ground state and the first excited state in ^{14}O, respectively. Until a separate measurement of the ratio $\sigma_{n_1}/\sigma_{n_0}$ is performed we cannot compare our measurement to their results.

We now use our experimental Γ_γ to infer typical stellar conditions for the operation of the "hot" CNO cycle. It is useful to define the cross section factor $S(E)$ (Ref. 7)

$$S(E) = E\sigma(E)\exp\left(\frac{E_G}{E}\right)^{1/2} ,$$

where $\sigma(E)$ is the ^{13}N(p,γ) cross section, and E is the proton energy in the center of mass. The Gamow energy is

$$E_G = (2\pi\alpha Z_{^{13}\mathrm{N}} Z_p)^2 (Mc^2/2) ,$$

where α is the fine structure constant; $Z_{^{13}\mathrm{N}}$ and Z_p are the atomic numbers of the two interacting particles; and M is the reduced mass.

The S-factor should be a slowly varying function of the energy far from reaction resonances,[7,1] since the strong energy dependences of the Coulomb and s-wave centrifugal barrier penetrabilities have been removed. In terms of the S-factor, the stellar reaction rate is[7]

$$\langle\sigma v\rangle = \left(\frac{8}{M\pi}\right)^{1/2} \frac{1}{(kT)^{3/2}} \times \int_0^\infty S(E)\exp\left[-\left(\frac{E_G}{E}\right)^{1/2} - \frac{E}{kT}\right] dE . \quad (1)$$

If $S(E)$ is a relatively smooth function of the energy, the integrand has a sharp peak at the maximum of the exponential, $E_0 = (E_G^{1/2}kT/2)^{2/3}$. The $1/e$ full-width of this peak is given by $\Delta E_0 = 4(E_0 kT/3)^{1/2}$.[7] At $T = 10^9$ K $E_0 = 440$ keV and $\Delta E_0 = 450$ keV. To compute the ^{13}N(p,γ)^{14}O reaction rate for temperatures of interest, $T < 10^9$ K, it is only necessary to determine the proton capture S factor for energies $E < 1000$ keV.

If only s-wave protons contribute to the (p,γ) reaction in this energy range (implying a unique S=1 reaction channel spin) the S-factor can be written as[14,11]

$$S(E) = S_R(E) + S_{\mathrm{DC}}(E) + 2\sqrt{S_R(E)S_{\mathrm{DC}}(E)}\cos[\delta_R(E)] ,$$

where $S_R(E)$ and $S_{\mathrm{DC}}(E)$ are the resonance and direct capture contributions to the reaction cross section, respectively. The phase of the interference is given by the difference in phase shifts between the resonance and direct capture s waves, and is equal to the resonance phase shift δ_R

$$\delta_R(E) = \tan^{-1}\left(\frac{\Gamma(E)}{2(E - E_R)}\right) .$$

The direct capture amplitude interferes constructively below the resonance and destructively above. This interference pattern has been observed in the analogous $s \rightarrow p$ direct capture transition in ^{12}C(p,γ)^{13}N.[14]

The resonance contribution $S_R(E)$ is described by a single level Breit-Wigner expression

$$S_R(E) = \frac{\pi\hbar^2}{2M}\frac{2J_R+1}{(2J_t+1)(2J_p+1)}\frac{\Gamma_p(E)\Gamma_\gamma(E)}{(E-E_R)^2+\Gamma^2/4} .$$

J_R, J_t, and J_p are the resonance, target and projectile spins, respectively, and E_R is the resonance energy. The energy dependence of the widths is given by[11]

$$\Gamma_p(E) = \Gamma_p(E_R)\frac{P_0(E)}{P_0(E_R)}$$

and

$$\Gamma_\gamma(E) = \Gamma_\gamma(E_R)\left(\frac{Q_0+E}{Q_0+E_R}\right)^3 ,$$

where Q_0 is the ground state Q value for ^{13}N(p,γ), Q_0=4.27 MeV, and $P_0(E)$ is an s-wave Coulomb penetrability evaluated at a channel radius of R=4 fm. (The

dependence on R largely cancels when we take the ratio of penetrabilities.) $S_R(E)$ is therefore specified by the experimental values of $\Gamma_\gamma = 2.6 \pm 1.3$ eV, and $\Gamma = \Gamma_p = 38.1 \pm 1.8$ keV.

The direct capture contribution to ^{13}N(p,γ) can be inferred from existing measurements[48] of the ^{13}C(p,γ_1) reaction to the 2.31 MeV, $J^\pi = 0^+$ state in ^{14}N, the isospin analog of the ^{14}O ground state. [The resonance contribution, of course, cannot be inferred from the ^{13}C(p,γ_1) data, since the $E1$ transition from the $J^\pi = 1^-$, T=1 resonance to the 0^+, T=1 analog state in ^{14}N is isospin forbidden.] The ^{13}C(p,γ_1) data are well described by the expression

$$S_{DC}(E) = C^2S \times S_{DC}^{theo}(E) ,$$

where C^2 is the isospin Clebsch-Gordan coefficient that couples the projectile and target to the final state, S is the final state spectroscopic factor, and S_{DC}^{theo} is the theoretical direct capture S factor. Assuming that the spectroscopic factor for the ground state of ^{14}O is the same as for its isospin analog in ^{14}N, the direct capture contribution to ^{13}N(p,γ) can be obtained by scaling the ^{13}C(p,γ_1) data by the ratio of the theoretical direct capture S factors for ^{13}N(p,γ_0) and ^{13}C(p,γ_1), and taking into account the isospin Clebsch-Gordan coefficients. We calculated the ratio of theoretical direct capture S factors following the formalism of Rolfs,[49] assuming a transition from an initial s-wave continuum state to a final nuclear bound state with the emission of γ radiation. The initial wave function was computed using a Coulomb plus hard sphere nuclear potential. (We used $R_0 = r_0[(A_t)^{1/3} + (A_p)^{1/3}]$, with $r_0 = 1.45$ fm; A_t and A_p are the masses of the target and projectile in atomic mass units.) The final $1p_{1/2}$ bound-state wave function was computed using a Coulomb plus Woods-Saxon nuclear potential, with diffuseness $a = 0.65$ fm, charge and mass radii $r_0 = 1.22$ fm, and spin-orbit term $V_{so} = 20.5$ MeV. The depth of the Woods-Saxon potential was adjusted to reproduce the binding energy of the final nuclear state.

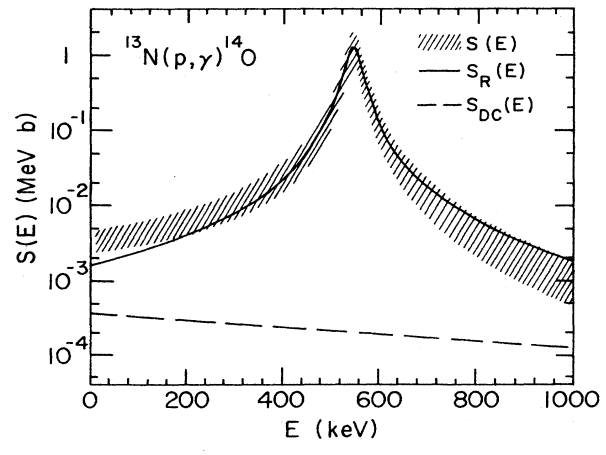

FIG. 13. Empirical S-factor for the ^{13}N$(p,\gamma)^{14}$O reaction as a function of center-of-mass energy. The band indicates the one standard deviation uncertainty in the computation of $S(E)$, due to the uncertainty in Γ_γ.

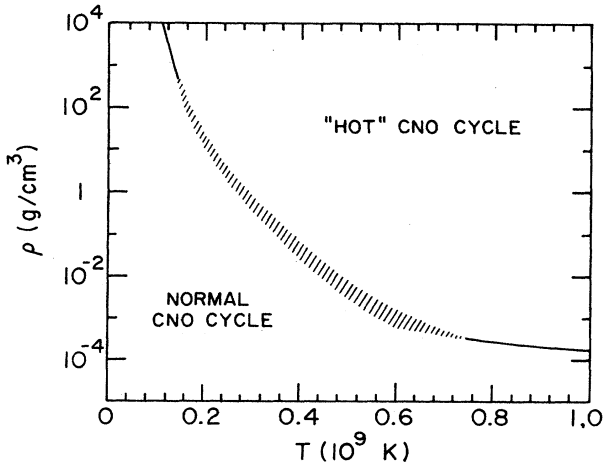

FIG. 14. Temperature and density conditions for the operation of the "hot" CNO cycle. A hydrogen fraction X_H =0.77 is assumed (Ref. 21). The band represents the $\pm 1\sigma$ uncertainty in the ^{13}N(p,γ) reaction rate, due to the uncertainty in Γ_γ.

From these calculations we extracted an average ratio

$$\frac{[S_{DC}^{theo}(E)]_{^{13}C(p,\gamma_1)}}{[S_{DC}^{theo}(E)]_{^{13}N(p,\gamma_0)}} = 0.77$$

which remained constant within $\approx$10% for $E_p < 1000$ keV. [The direct capture cross section for ^{13}N(p,γ) is larger because the more loosely bound ^{14}O ground state has a better radial overlap with the s-wave scattering-state wave function than does the more tightly bound level in ^{14}N.] The direct capture contribution to ^{13}N(p,γ) can be parametrized as

$$S_{DC}(E) = 0.368 \ \exp(-1.088 \times 10^{-3}E)$$

with E in keV and $S_{DC}(E)$ in keV b.

Figure 13 shows the resulting ^{13}N(p,γ) S factor. The uncertainty in the computation is dominated by the error in Γ_γ. Using this experimentally determined S factor, we can compute the reaction rate as a function of the temperature by numerically integrating Eq. (1). The "hot" CNO cycle is fully operational when the rate of energy generation of the cycle is dominated by the β decay of the oxygen isotopes.[21] Figure 14 shows the conditions of stellar temperature and density under which the proton capture rate on ^{13}N or ^{14}N, whichever is slowest, becomes faster than the sum of the β-decay rates for ^{14}O and ^{15}O. The ^{14}N(p,γ) rate was taken from Ref. 50. We have thus obtained a description of the stellar environments where the "hot" CNO cycle can operate.

ACKNOWLEDGMENTS

The help of D. R. Balsley in fabricating the implanted ^{12}C target is gratefully acknowledged. We also thank K. A. Snover for helpful discussions at different stages of this work, and M. Khandaker and M. M. Hindi for collaborating with us in the initial phases of the experiment. This research was supported in part by the U.S. Department of Energy.

*Present address: Physics Division, Argonne National Laboratory, Argonne, IL 60439.

[1] D.D. Clayton, *Principles of Stellar Evolution and Nucleosynthesis* (McGraw-Hill, New York, 1968).

[2] W.S. Rodney and C. Rolfs, in *Essays in Nuclear Astrophysics*, edited by C.A. Barnes, D.D. Clayton, and D.N. Schramm (Cambridge University Press, New York, 1982), p. 171.

[3] G.R. Caughlan and W.A. Fowler, Astrophys. J. **136**, 453 (1962).

[4] F. Hoyle and W.A. Fowler, in *Quasi-Stellar Sources and Gravitational Collapse*, edited by I. Robinson, A. Schild, and E.L. Schucking (University of Chicago Press, Chicago, 1965), p. 17.

[5] J. Audouze, J.W. Truran, and B.A. Zimmerman, Astrophys. J. **184**, 493 (1973).

[6] R.K. Wallace and S.E. Woosley, Astrophys. J. Suppl. Ser. **45**, 389 (1981).

[7] W.A. Fowler, G.R. Caughlan, and B.A. Zimmerman, Annu. Rev. Astron. Astrophys. **5**, 525 (1967).

[8] G.J. Mathews, R.W. Bauer, R.C Haight, and K.E. Sale, in *Proceedings of the Accelerated Radioactive Beams Workshop*, edited by L. Buchmann and J.M. D'Auria (TRIUMF, Vancouver, Canada, 1985), p. 241.

[9] J.K.P. Lee, in *Proceedings of the Accelerated Radioactive Beams Workshop*, edited by L. Buchmann and J.M. D'Auria (TRIUMF, Vancouver, Canada, 1985), p. 77.

[10] M. Arnould *et al.*, in *Proceedings of the International Symposium on Heavy Ion Physics and Nuclear Astrophysical Problems*, edited by S. Kubono, M. Ishihara, and T. Nomura (World Scientific, Singapore, 1989), p. 287.

[11] C. Funck and K. Langanke, Nucl. Phys. **A464**, 90 (1987).

[12] P. Parker, in *Proceedings of the Accelerated Radioactive Beams Workshop*, edited by L. Buchmann and J.M. D'Auria (TRIUMF, Vancouver, Canada, 1985), p. 144.

[13] D.F. Hebbard and J.L. Vogl, Nucl. Phys. **21**, 652 (1960).

[14] C. Rolfs and R.E. Azuma, Nucl. Phys. **A227**, 291 (1974).

[15] In ^{12}C$(p,\gamma)^{13}$N there are no subthreshold bound states that make significant contributions to the low-energy cross section [as is the case of ^{12}C$(^4$He$,\gamma)^{16}$O (Ref. 51)], and the tail of the next resonance at E=1699 keV, Γ = 62 keV, is negligible (see, for example, Ref. 14 and references therein).

[16] F. Ajzenberg-Selove, Nucl. Phys. **A449**, 1 (1986).

[17] T.E. Chupp, R.T. Kouzes, A.B. McDonald, P.D. Parker, T.F. Wang, and A.J. Howard, Phys. Rev. C **31**, 1023 (1985).

[18] T.F. Wang, Ph.D. thesis, Yale University, 1986.

[19] B.A. Brown, private communication.

[20] A.P. Zucker, B. Buck, and J.B. McGrory, Phys. Rev. Lett. **21**, 39 (1968).

[21] G.J. Mathews and F.S. Dietrich, Astrophys. J. **287**, 969 (1984).

[22] K. Langanke, O.S. van Roosmalen, and W.A. Fowler, Nucl. Phys. **A435**, 657 (1985); **A446**, 750 (1985).

[23] F.C. Barker, Aust. J. Phys. **38**, 657 (1985).

[24] P. Descouvemont and D. Baye, in *Proceedings of International Symposium on Heavy Ion Physics and Nuclear Astrophysical Problems*, edited by S. Kubono, M. Ishihara, and T. Nomura (World Scientific, Singapore, 1989), p. 97.

[25] E.K. Warburton and J. Weneser, in *Isospin in Nuclear Physics*, edited by D.H. Wilkinson (North-Holland, Amsterdam, 1969), p. 173.

[26] R.E. Marrs, E.G. Adelberger, K.A. Snover, and M.D. Cooper, Phys. Rev. Lett. **35**, 202 (1975).

[27] R.G. Thomas, Phys. Rev. **88**, 1109 (1952).

[28] D. Kurath, Phys. Rev. Lett. **35**, 1546 (1975).

[29] E.G. Adelberger and A.B. McDonald, Nucl. Phys. **A145**, 497 (1970).

[30] Prepared by Micromatter Co., East Sound, Washington.

[31] Puratronic gold foil, supplied by Johnson Matthey Inc., Aesar Group, Seabrook, New Hampshire.

[32] P.B. Fernandez, Ph.D. thesis, University of Washington, 1989.

[33] E.G. Adelberger, A.B. McDonald, and C.A. Barnes, Nucl. Phys. **A124**, 49 (1969).

[34] W.R. Nelson, H. Hirayama, and D.W.O. Rogers, Stanford Linear Accelerator Center Report 265, 1985.

[35] G.R. Satchler, *Direct Nuclear Reactions* (Oxford University Press, New York, 1983).

[36] R.M. Steffen and K. Alder, in *The Electromagnetic Interacion in Nuclear Spectroscopy*, edited by W.D. Hamilton (North-Holland, Amsterdam, 1975), p. 505.

[37] J.W. Noé, D.P. Balamuth, and R.W. Zurmühle, Phys. Rev. C **9**, 132 (1974).

[38] In the single-step two-nucleon reaction model, T=1 states in ^{14}N are populated through the ^{12}C$(^3$He$,p)$ reaction via the transfer of a J=0, T=1 quasideuteron. If the protons are detected at 0 deg, only the M=0 substates of the ^{14}N state will be populated.

[39] In contrast, the ^{12}C$(^3$He$,p)$ reaction populating T=0 bound states shows a significant compound nucleus contribution, even for $E_{^3\mathrm{He}}$ = 20 MeV (Refs. 52 and 53). Apparently direct quasideuteron (J=0, T=1) transfer is favored over deuteron (J=1, T=0) transfer, see Ref. 53.

[40] D.P. Balamuth, J.M. Lind, K.C. Young, Jr., and R.W. Zurmühle, Nucl. Phys. **A290**, 65 (1977).

[41] D.E. Alburger, D.P. Balamuth, J.M. Lind, L. Mulligan, K.C. Young, Jr., R.W. Zurmühle, and R. Middleton, Phys. Rev. C **17**, 1525 (1978).

[42] S. DeBenedetti, *Nuclear Interactions* (Wiley, New York, 1964).

[43] M.E. Rose, Phys. Rev. **91**, 610 (1953).

[44] C.D. Zerby and H.S. Moran, Nucl. Instrum. Methods **14**, 115 (1961).

[45] M.J.L. Yates, Nucl. Instrum. Methods **23**, 13 (1963).

[46] P. Aguer, G. Bogaert, M. Kious, V. Landré, A. Lefebvre, J.P. Thibaud, F. Beck, and A. Huck, in *Proceedings of the International Symposium on Heavy Ion Physics and Nuclear Astrophysical Problems*, edited by S. Kubono, M. Ishihara, and T. Nomura (World Scientific, Singapore, 1989),

p. 107.
[47]T.F. Wang, K.E. Rehm, S.J. Sanders, C.N. Davids, B.G. Glagola, R. Holzmann, W.C. Ma, P.V. Magnus, P.D. Parker, and M. Smith, Bull. Am. Phys. Soc. Ser. II **33**, 1564 (1988).
[48]R.E. Azuma, J.D. King, J.B. Vise, J. Görres, H.P. Trautvetter, C. Rolfs, and A.E. Vlieks, in *Proceedings of the Accelerated Radioactive Beams Workshop*, edited by L. Buchmann and J.M. D'Auria (TRIUMF, Vancouver, Canada, 1985), p. 70.
[49]C. Rolfs, Nucl. Phys. **A217**, 29 (1973).
[50]W.A. Fowler, G.R. Caughlan, and B.A. Zimmerman, Annu. Rev. Astron. Astrophys. **13**, 69 (1975).
[51]T.A. Tombrello, S.E. Koonin, and B.A. Flanders, in *Essays in Nuclear Astrophysics*, edited by C.A. Barnes, D.D. Clayton, and D.N. Schramm (Cambridge University Press, New York, 1982), p. 233.
[52]B. Heusch and A. Gallmann, Phys. Rev. C **7**, 1810 (1973).
[53]B. Heusch, F. Haas, R.M. Freeman, and A. Gallmann, Phys. Rev. C **15**, 1196 (1977).